



CHALMERS

Chalmers Publication Library

Coastal Sea Ice Detection Using Ground-Based GNSS-R

This document has been downloaded from Chalmers Publication Library (CPL). It is the author's version of a work that was accepted for publication in:

IEEE Geoscience and Remote Sensing Letters (ISSN: 1545-598X)

Citation for the published paper:

Strandberg, J. ; Hobiger, T. ; Haas, R. (2017) "Coastal Sea Ice Detection Using Ground-Based GNSS-R". IEEE Geoscience and Remote Sensing Letters, vol. 14(9), pp. 1552-1556.

<http://dx.doi.org/10.1109/LGRS.2017.2722041>

Downloaded from: <http://publications.lib.chalmers.se/publication/251083>

Notice: Changes introduced as a result of publishing processes such as copy-editing and formatting may not be reflected in this document. For a definitive version of this work, please refer to the published source. Please note that access to the published version might require a subscription.

Chalmers Publication Library (CPL) offers the possibility of retrieving research publications produced at Chalmers University of Technology. It covers all types of publications: articles, dissertations, licentiate theses, masters theses, conference papers, reports etc. Since 2006 it is the official tool for Chalmers official publication statistics. To ensure that Chalmers research results are disseminated as widely as possible, an Open Access Policy has been adopted. The CPL service is administrated and maintained by Chalmers Library.

(article starts on next page)

Coastal sea ice detection using ground-based GNSS-R

Joakim Strandberg, *Student Member, IEEE*, Thomas Hobiger, *Member, IEEE*, and Rüdiger Haas.

Abstract

Determination of sea ice extent is important both for climate modeling and transportation planning. Detection and monitoring of ice is often done by SAR imagery, but mostly without any ground truth. For the latter purpose, robust and continuously operating sensors are required. We demonstrate that signals recorded by ground-based GNSS receivers can detect coastal ice coverage on nearby water surfaces. Beside a description of the retrieval approach, we discuss why GNSS reflectometry is sensitive to the presence of sea ice. It is shown that during winter seasons with freezing periods, GNSS-R analysis of data recorded with a coastal GNSS installation clearly shows the occurrence of ice in the bay where this installation is located. Thus, coastal GNSS installations could be promising sources of ground truth for sea ice extent measurements.

Index Terms

GNSS-R, sea ice, Global Navigation Satellite System, reflectometry, SNR, inverse modeling

I. INTRODUCTION

Measurements of sea ice extent provide important input for climate models and monitoring [1] as well as for studies of ecological systems [2]. They also contribute crucial information for human activities such as marine transportation in the arctic [3]. Usually, the ice extent is measured with SAR imaging techniques [4]. However, as ice and water can have very similar signatures on SAR images [5], distinguishing the two states can be difficult. Furthermore, ice growth starts near the coastline [6] where the resolution of satellite image data is often coarse. Under these conditions, ground truth data are important as they can be used as reference for SAR measurements, as well as provide long term reliable time series for climate research.

Reflectometry measurements of signals from Global Navigation Satellite Systems (GNSS) have been used for several years to observe sea level variations [7], soil moisture [8], and other geophysical parameters [9], [10]. GNSS multipath is a signal of opportunity which for high precision GNSS applications is usually considered an error source [11], but it contains useful geometric and physical information and is freely available for many stations around the world [12].

The authors are with the Department of *Space, Earth and Environment*, Chalmers University of Technology. *Corresponding author: Joakim Strandberg (joakim.strandberg@chalmers.se)*

Manuscript received December ???, 2016.

An earlier attempt using ground-based GNSS-reflectometry could not significantly detect the presence of sea ice [13]. However, the primary goal of the study was to measure ocean tides in the arctic and sea ice detection was only done by comparing measured sea surface heights with heights predicted from an ocean model. While the authors briefly discuss that high coherence of the reflected signals and the presence of ice coincides they do not draw any conclusions on how to use it to accurately detect ice. In the following sections we introduce a novel approach of detecting sea ice with common geodetic GNSS receivers, based on inverse modeling of signal to noise ratio (SNR) patterns of the reflected signals.

II. EXTRACTION OF REFLECTOR PROPERTIES FROM SNR MEASUREMENTS

Normally GNSS receivers log, beside code and carrier phase observations, also the SNR. Assuming that the acquisition is affected by interference coming from a single horizontal reflecting surface, the SNR time series of a satellite passage can be separated into a slowly varying and a high frequency part. The latter, referred to as δSNR , varies with elevation ε as

$$\delta\text{SNR} = A \cos\left(\frac{4\pi h}{\lambda} \sin \varepsilon + \varphi\right), \quad (1)$$

where λ denotes the carrier wavelength, according to [14]. The height of the antenna above the reflector is denoted by h , and φ is a constant phase offset. The elevation angles ε are already corrected for atmospheric bending in accordance to the empirical model described in [15] and thus allow to invert SNR interference information with the correct geometry at the GNSS ground station. [16] extended the model including properties of the reflection, leading to

$$\begin{aligned} \delta\text{SNR} = & \left[C_1 \sin\left(\frac{4\pi h}{\lambda} \sin \varepsilon\right) + C_2 \cos\left(\frac{4\pi h}{\lambda} \sin \varepsilon\right) \right] \\ & \times \exp(-4k^2\gamma \sin^2 \varepsilon), \end{aligned} \quad (2)$$

where k is the wave number, C_1 and C_2 determine the amplitude and the phase of the sinusoid, and γ relates to properties of the reflecting surface. This functional model is used in a non-linear least-squares adjustment process to retrieve h , C_1 , C_2 , and γ . Table I describes the parametrization of the variables that are fitted in the inversion process. The actual inversion is performed as a combined solution, including all GPS and GLONASS data available at a site. As described by [16], data from a period of three days are processed together and the results of the middle day are then used for further analysis. This sliding window processing scheme allows to obtain stable, smooth and continuous time series of the target parameters.

One can expect that the strength of the interfering signal changes depending on the shape and electromagnetic properties of the reflector. Thus, the estimated amplitudes $A = \sqrt{C_1^2 + C_2^2}$ will contain information about these properties. However, one has to be aware that A varies also with satellite system and frequency, which makes it difficult to interpret the obtained values in an unbiased sense. The phase offset $\varphi = \arctan\left(\frac{C_1}{C_2}\right)$, which is the main parameter for GNSS-R based soil moisture studies [8], is not considered in the following as no significant relation to ice state was found.

In contrast, the parameter γ turns out to be better suited for deducing the physical state of the reflecting water surface. In theory, the coherence of the reflected signal decays with satellite elevation and roughness of the reflecting

TABLE I
PARAMETERIZATION OF THE INVERSE MODEL

Parameter	Temporal resolution
C_1, C_2	One value for each GNSS and frequency per 72 h ^a
γ	One value per 72 h ^a
h	Spline function with nodes every 2 hours

^aData are taken with overlap, effectively leading to one parameter value per 24 h.

surface as the last term in Eq. (2): $\exp(-4k^2\gamma\sin^2\varepsilon)$, where γ corresponds to the height variance of the reflector [17]. However, there are various unmodeled elevation-dependent effects, such as those related to the dielectric properties of the reflector and the antenna gain [18], which impact the interference amplitude and therefore the damping of the oscillations. Therefore, the retrieved parameter γ will not directly correspond to the roughness of the surface. Instead it will have contributions from all these effects, and thus interpreting γ as variance of the surface is inadvisable. But as the antenna gain pattern is constant over time, and both roughness and dielectric properties change upon ice formation, it is expected that γ will also change significantly when ice is formed. Thus, following the approach of [16], inversion of SNR data from coastal GNSS-R sites is expected to provide not only time series of sea surface heights, but also information about whether the water surface is liquid or frozen.

III. EXPERIMENT SETUP

SNR data from GNSS signals were collected at the permanent coastal research installation GTGU at the Onsala Space Observatory, Sweden, which consists of a standard LEICA AR25 RHCP antenna and a LEICA GRX1200 receiver. The GNSS receiver was configured to collect data of both GPS and GLONASS with 1 Hz sampling frequency. For the subsequent GNSS-R data processing, a sky mask was used to allow only data between 70° and 260° in azimuth and below 15° elevation, which ensures that only tracks from the sea surface are used in the processing.

Coherent multipath signals are effectively collected from an area often approximated by the first Fresnel zone [19], with the specular point in the center. Considering that the combination of GPS and GLONASS leads to many different ground tracks, the area around the GNSS installation is sampled well, both in space and time.

During the winters of 2012 and 2013, regular visual inspection confirmed that the bay where GTGU is located was completely covered by ice during certain periods (see Fig. 1a). This allows for studying the effect of sea ice on reflected GNSS signals. The winters of 2014 and 2015 were ice-free, and thus are only used as a reference for open water conditions. Finally, in 2016 the temperatures dropped only for a shorter period, not enough to freeze the bay completely, but only leading to the formation of ice floes (Fig. 1c).

Complementary to visual inspection, a meteorological sensor was available in proximity of the test site. In addition, precipitation and snow depth data for the above mentioned periods were collected from the official Swedish Meteorological and Hydrological Institute (SMHI) weather station Onsala D, which is located roughly 2 km away from the GNSS station. For validation purposes, ice charts provided by SMHI were also used (c.f. Fig. 1b).

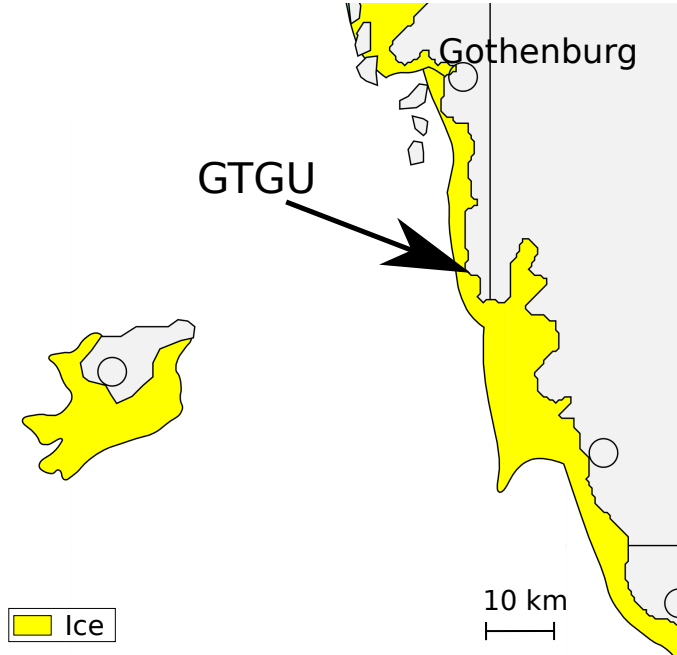
a) GTGU, 6 February 2012**b) Ice map, 6 February 2012****c) Coastal environment at Onsala Space Observatory, 22 January 2016**

Fig. 1. a) Photo of the GTGU installation on February 6, 2012. At this time the bay was completely covered by sea ice. b) Ice map provided by SMHI for February 6, 2012, with the location of the GTGU GNSS installation marked. c) Panorama of the coastal environment outside Onsala Space Observatory on January 22, 2016, when the sea was partially covered by ice.

IV. RESULTS

The damping parameter γ was extracted from SNR data recorded in the winter seasons of 2012 and 2013 using the inversion algorithm described in Section II. As mentioned before, the damping is also affected by different parameters which are not related to the surface characteristics. Thus, the damping coefficients were normalized by the mean damping value of the ice-free winter in 2015, providing a relative damping factor $\gamma_{\text{rel}} = \gamma/\gamma_{2015}$. This factor can be expected to contain information related to changes of the physical properties of the reflector. It has been confirmed that during ice-free periods the relative damping stays close to 1.0 and varies within the range $\gamma_{\text{rel}} \in [0.92, 1.09]$. Any significantly smaller value of γ_{rel} is thus expected to indicate a state transition as both the change in permittivity and the smoother surface of newly formed ice increases the power of the coherent reflections

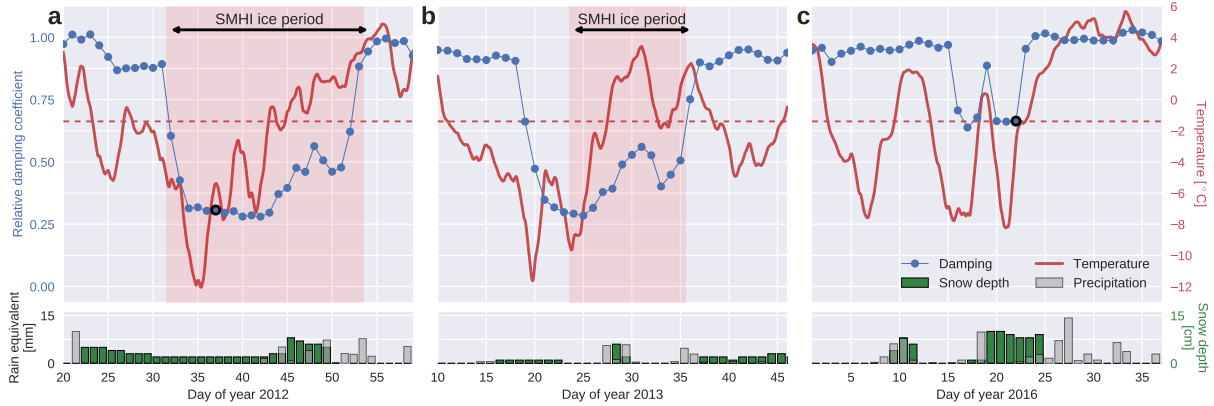


Fig. 2. Time series of damping coefficients (blue dots) and a 12 h running mean of the air temperature (red line) for periods of the winters of a: 2012, b: 2013 and c: 2016. The damping coefficient is relative to the average value of the ice-free winter of 2015. The average freezing temperature of sea water near GTGU, i.e. -1.4°C , is marked for reference, and the shaded periods correspond to the times when ice maps by SMHI reports ice coverage outside Onsala. The two black circles correspond to the dates when the photos of Figure 1 were taken. The lower plots show the rain equivalent of the snow/rain fall (gray), as well as the accumulated snow depth (green).

at higher elevations [18], i.e. less damping.

Time series of the resulting parameter are presented in Fig. 2, together with temperature and precipitation data from the nearby meteorological stations. It can be noticed that around day of year (DOY) 32, 2012, the relative damping parameter decreases by more than 60%. After this sudden drop of γ_{rel} , the damping stays at a low value for 20 days. Photos taken during this period reveal that the bay was completely covered by a sheet of flat ice (Fig. 1a). The decrease in damping is much larger than the normal variability during ice-free periods, which indicates that the damping coefficient is affected by the ice formation.

Other than visual inspection, one can also conclude on the presence of ice by studying temperature time series. The exact freezing point of sea water depends on the salinity. From time series provided by SMHI, the average salinity in surface layers of sea outside GTGU is 25‰, indicating a freezing temperature of seawater of -1.4°C [20]. Since no water temperature measurements were available, we used locally recorded air temperature as a proxy, considering that there is a time lag between water and air temperatures [21]. As presented in Fig. 2, the air temperature is below the freezing temperature of sea water for several days before the relative damping γ_{rel} drops significantly. The effect of water as a temperature buffer, i.e. a time lag between the air temperature decrease and the freezing [21], is thus clearly visible in the figure.

Ice maps by SMHI were also used for validation. The areas shaded in red in Fig. 2 correspond to the time periods when the ice maps indicate ice of any kind on the sea west of GTGU (see Fig. 1). For the winter of 2012, the reported ice coverage corresponds closely in time to the period of decreased signal damping. The slight discrepancy at the end of the ice period can most likely be explained by the low spatial resolution of the ice charts.

The pattern seen in 2012 repeats in the time series for 2013 in Fig. 2. Again, a few days after the temperature drops below the freezing point for sea water, the damping coefficient also decreases significantly (cf. DOY 19,

2013), indicating that there was ice in the bay at that time. For 2013, the ice maps do not show any ice coverage in the area until DOY 24, a few days after the damping indicates ice. No ice coverage in the area has been reported after DOY 36, coinciding with the damping returning to normal values. Differences between the epochs when the damping drops and when the ice maps report ice coverage can also be explained by local topography and the coarse resolution of the maps. Especially, as the bay at the observatory is sheltered from waves by a few islets, ice can form there earlier than on the surrounding open sea.

In both years, after a clear period of ice the damping increased slightly, at day of year 44 and 27 respectively, following on events of snowfall. This suggests that snow which had piled up on the sea ice changing the surface properties, thus increasing the damping factor γ_{rel} . Later, as the temperature rises the snow melts, which temporarily changes the properties of the surface before the underlying ice also melts and the damping returns to pre-ice levels again.

During the winter of 2016 the weather conditions were not cold enough to freeze the bay completely. However, there was an intermediate state with pancake ice and frazil ice in-between (Fig. 2c). Even though the bay did not completely freeze, there is still some variability visible in the damping time series. As presented in Fig. 2, the damping drops by around 30% during the winter of 2016. This is less than for the winters of 2012 and 2013 but is still a significant change, showing that the obtained damping parameter is sensitive even to partial freezing.

The correlation between damping and presence of ice is also evident from Fig. 3 which depicts a scatter plot of mean temperature versus relative damping from GNSS-R for the winters of 2012 and 2013, for which freezing occurred. However, as noted previously, there is a time lag between the drop in temperature and in damping in Fig. 2, since it takes some time for the sea water to freeze. Therefore, the temperature in Fig. 3 is offset by the time lag that maximizes the correlation between the damping and the temperature. These time lags are found to be 8.2 days for 2012, and 8.8 days for 2013. The figure depicts a clear population of points in the upper right corner corresponding to ice-free days, and a spread of points stretching to the lower left corner of the plot containing the days where ice covered the bay. In between there is a transition zone containing damping values related to snow-covered ice, floating ice sheets and partially frozen water surfaces. Especially worth noticing is that relative damping coefficients above 0.9 only occur for temperatures above -1.4°C and that the low values only occur for negative temperatures, strongly supporting the conclusion that damping is a good indicator for the presence of ice.

V. ICE-RELATED INFORMATION FROM OTHER GNSS-R PARAMETERS

As already mentioned in Section II also the other estimated parameters (cf. Tab. I) might be useful for studying the freezing state of water nearby GNSS installations.

Concerning the use of interference amplitude information, one has to be aware that signal strength varies with satellite system and frequency, which makes it necessary to estimate individual values for each combination of GPS and GLONASS as well as L1 and L2. In order to avoid signatures of site-specific characteristics, relative amplitudes $A_{\text{rel}} = A/A_{\text{ice free}}$ were derived from the GTGU inversion results, where $A_{\text{ice free}}$ was computed for each combination of satellite system and frequency. The upper plots in Fig. 4 depict time series of these relative amplitudes with the period of ice marked. Periods of ice coverage can be identified by higher values of A_{rel} . However, compared

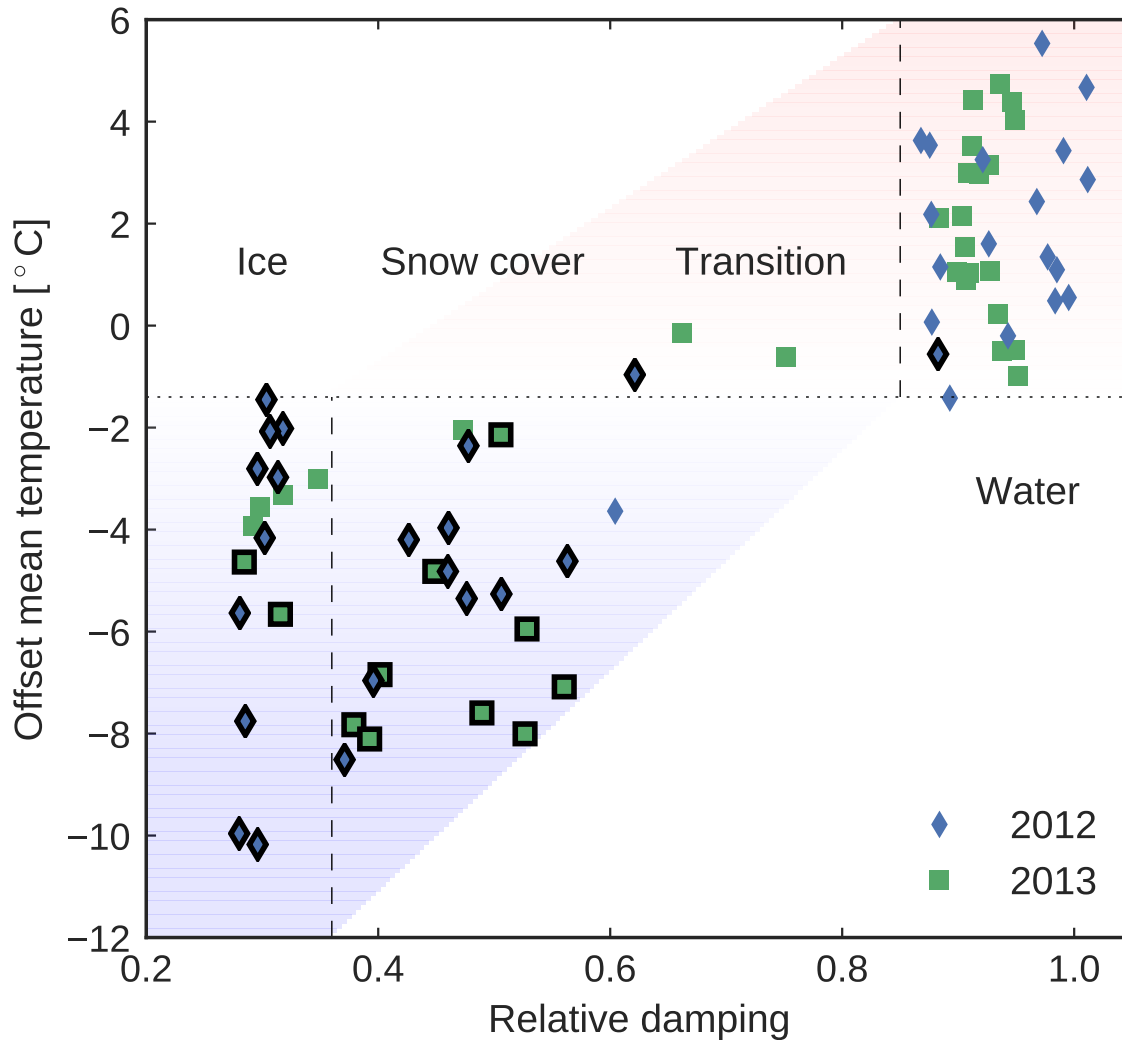


Fig. 3. Scatter plot of daily mean air temperatures and relative damping coefficients. The time of the temperature readings in the figure is offset by the time lag that gives the maximum correlation between the damping and temperature time series: 8.2 days for 2012, and 8.8 days for 2013. A black border indicates dates when the SMHI ice maps show ice at Onsala. The color of the shading is determined by temperature.

to Fig. 2 the response of the amplitude is less pronounced, especially during the transition period. Moreover, the magnitude of the amplitude change is depending on satellite system and frequency and reveals different patterns, in particular for the 2013 study period. Thus, it can be concluded that the estimated amplitudes contain some information about the freeze state, but in general can not be interpreted as straightforward as the damping values.

VI. SUMMARY AND DISCUSSION

The method presented in this paper, shows a clear capacity to detect the presence of ice around the GNSS station GTGU, using only the elevation dependent damping of SNR oscillations. The retrieved damping parameter time

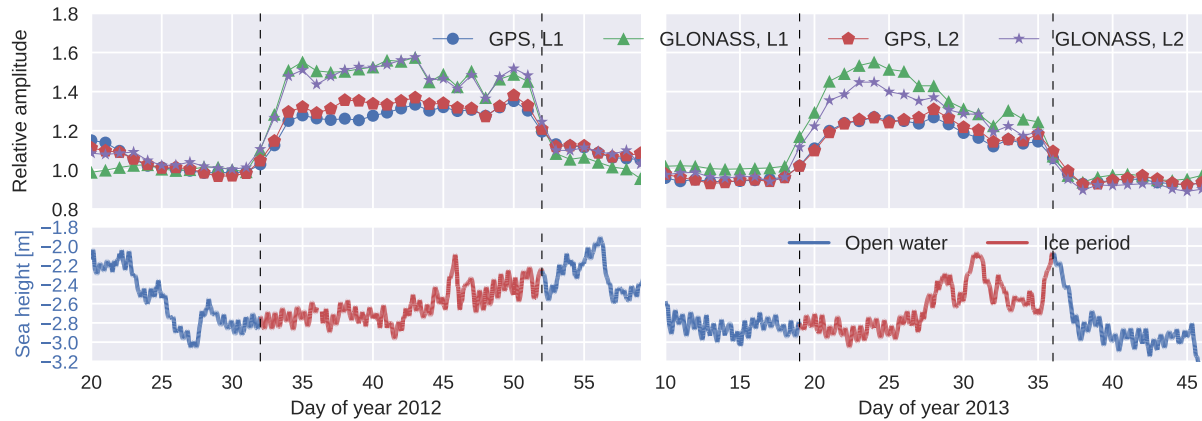


Fig. 4. Amplitudes (upper) and reflector height (lower) retrieved from the GNSS-R SNR data for the two winters with ice formation. The amplitude is relative to the ice-free winter of 2015. The color of the reflector height time series marks the occurrence of ice — red color indicates ice, and blue indicates open water — as retrieved from the damping parameter.

series, which contains contributions from both surface roughness and permittivity, contain a period of significantly lower values, coinciding with periods of sea ice in the measurement area. This distinct behavior of the signal in the presence of ice can be used for sea ice detection at coastal GNSS stations.

Automatic detection of sea ice is a promising new application of coastal GNSS reflectometry, especially since publicly distributed GNSS data are available for many stations around the world. Whereas most of them are located inland, several are close enough to the coast to be useful for ice detection. Our results also show that it is possible to detect even intermediate ice formation. Ice extent is usually monitored using active microwave sensors. For example SAR instruments have been proven to be very efficient for mapping ice velocity and ice types. Thus, ground-based GNSS-R can be seen as a complementary tool that provides data where those sensors usually have difficulties, i.e. close to the coast where existing networks of GNSS receiver could provide the along-coast extent of sea ice. In addition, GNSS sites are operating continuously over decades without instrumental changes. Hence, time series of coastal ice from GNSS-R can be used as ground-truth for the validation of satellite based sensors or as an additional constraining input to climatological models. This means that coastal GNSS-R has the potential to be a new source of information for oceanography, hydrology and climatology.

In general, the usage of the presented method opens up for new opportunities with ground-based GNSS-R. It is expected that the method presented here will be valuable also for other usages of GNSS-R. Also we can expect that if more effects are modeled, such as antenna gain and atmospheric effects, even more parameters could be retrieved with this method. Finally, the detection of ice from GNSS-R is useful as it opens up for further studies on the effect of ice on GNSS SNR patterns and signal quality. For example one could combine the knowledge of the presence of ice with the geometric information obtained from GNSS-R inversion and determine ice thickness or snow coverage. In order to illustrate this idea, we refer to the plots in the lower part of Fig. 4 which depict time-series of reflector height for the ice periods discussed before. Comparing these values with tide gauge data or other sensors would allow to draw further conclusions. Unfortunately, the co-located pressure tide gauge at Onsala

was not working properly during the study period 2012–2013 so that distinctions between ice and snow-coverage could only be made based on the information from visual inspection around the site. This drawback is expected to be overcome in the future, since a newly-built tide gauge and further additional sensors have been deployed recently in the proximity of the GTGU site, allowing for further ice and snow related studies during freeze-periods.

ACKNOWLEDGMENT

The International GNSS Service [12] is acknowledged for providing GNSS data and products. The GNSS equipment at Onsala was funded by the Adlerbertska Foundation and purchased through the Leica Geosystems ATHENA program. The precipitation data, ice charts and salinity data were retrieved from the archives of the SMHI [22].

REFERENCES

- [1] G. R. North, R. F. Cahalan, and J. A. Coakley, "Energy balance climate models," *Reviews of Geophysics*, vol. 19, no. 1, pp. 91–121, February 1981.
- [2] M. Perrette, A. Yool, G. Quartly, and E. Popova, "Near-ubiquity of ice-edge blooms in the arctic," *Biogeosciences*, vol. 8, no. 2, pp. 515–524, February 2011.
- [3] L. Pizzolato, S. E. L. Howell, C. Derksen, J. Dawson, and L. Copland, "Changing sea ice conditions and marine transportation activity in canadian arctic waters between 1990 and 2012," *Climatic Change*, vol. 123, no. 2, pp. 161–173, March 2014.
- [4] J. Askne and W. Dierking, "Sea ice monitoring in the arctic and baltic sea using sar," in *Remote Sensing of the European Seas*. Springer, 2008, pp. 383–398.
- [5] J. Karvonen, M. Simila, and M. Makynen, "Open water detection from baltic sea ice radarsat-1 sar imagery," *IEEE Geoscience and Remote Sensing Letters*, vol. 2, no. 3, pp. 275–279, July 2005.
- [6] M. Granskog, H. Kaartokallio, H. Kuosa, D. N. Thomas, and J. Vainio, "Sea ice in the baltic sea—a review," *Estuarine, coastal and shelf science*, vol. 70, no. 1, pp. 145–160, October 2006.
- [7] M. Martin-Neira, "A passive reflectometry and interferometry system (paris): Application to ocean altimetry," *ESA journal*, vol. 17, pp. 331–355, 1993.
- [8] K. M. Larson, E. E. Small, E. D. Gutmann, A. L. Bilich, J. J. Braun, and V. U. Zavorotny, "Use of gps receivers as a soil moisture network for water cycle studies," *Geophysical Research Letters*, vol. 35, no. 24, December 2008, 124405.
- [9] K. M. Larson, E. D. Gutmann, V. U. Zavorotny, J. J. Braun, M. W. Williams, and F. G. Nievinski, "Can we measure snow depth with GPS receivers?" *Geophysical Research Letters*, vol. 36, no. 17, September 2009, 117502.
- [10] N. Rodriguez-Alvarez, A. Camps, M. Vall-Ilossera, X. Bosch-Lluis, A. Monerris, I. Ramos-Perez, E. Valencia, J. F. Marchan-Hernandez, J. Martinez-Fernandez, G. Baroncini-Turricchia, C. Perez-Gutierrez, and N. Sanchez, "Land geophysical parameters retrieval using the interference pattern gnss-r technique," *IEEE Transactions on Geoscience and Remote Sensing*, vol. 49, no. 1, pp. 71–84, January 2011.
- [11] J. Braun, C. Rocken, and R. Ware, "Validation of line-of-sight water vapor measurements with gps," *Radio Science*, vol. 36, no. 3, pp. 459–472, May 2001.
- [12] J. M. Dow, R. Neilan, and C. Rizos, "The international gnss service in a changing landscape of global navigation satellite systems," *Journal of Geodesy*, vol. 83, no. 3-4, pp. 191–198, March 2009.
- [13] A. M. Semmling, G. Beyerle, R. Stosius, G. Dick, J. Wickert, F. Fabra, E. Cardellach, S. Rib, A. Rius, A. Helm, S. B. Yudanov, and S. d'Addio, "Detection of arctic ocean tides using interferometric gnss-r signals," *Geophysical Research Letters*, vol. 38, no. 4, February 2011, 104103.
- [14] Y. Georgiadou and A. Kleusberg, "On carrier signal multipath effects in relative gps positioning," *Manuscripta geodaetica*, vol. 13, no. 3, pp. 172–179, 1988.
- [15] G. Bennett, "The calculation of astronomical refraction in marine navigation," *Journal of the Institute of Navigation*, vol. 35, p. 255, 1982.
- [16] J. Strandberg, T. Hobiger, and R. Haas, "Improving gnss-r sea level determination through inverse modeling of snr data," *Radio Science*, vol. 51, no. 8, pp. 1286–1296, August 2016.

- [17] P. Beckmann and A. Spizzichino, *The scattering of electromagnetic waves from rough surfaces*. Artech House, Inc., 1987.
- [18] F. G. Nievinski and K. M. Larson, "Forward modeling of gps multipath for near-surface reflectometry and positioning applications," *GPS Solutions*, vol. 18, no. 2, pp. 309–322, 2014. [Online]. Available: <http://dx.doi.org/10.1007/s10291-013-0331-y>
- [19] S. Jin, E. Cardellach, and F. Xie, *GNSS remote sensing*. Springer, 2014.
- [20] K. Fujino, E. Lewis, and R. Perkin, "The freezing point of seawater at pressures up to 100 bars," *Journal of Geophysical research*, vol. 79, no. 12, pp. 1792–1797, April 1974.
- [21] B. Rodhe, "On the relation between air temperature and ice formation in the baltic," *Geografiska Annaler*, vol. 34, pp. 175–202, 1952.
- [22] "Smhi open data," SMHI. [Online]. Available: <http://opendata-catalog.smhi.se/explore/>